10

Faraday effect in three-periodic bigyrotropic photonic crystals

© N.N. Dadoenkova[1], I.A. Glukhov[1,2,3], I.S. Panyaev[1,2], D.G. Sannikov[1,2], Yu.S. Dadoenkova[4]

[1] Galkin Donetsk Institute for Physics and Engineering,
Donetsk, Russia
[2] Ulyanovsk State University,
Ulyanovsk, Russia
[3] Kotel'nikov Institute of Radio Engineering and Electronics (Ulyanovsk Branch), Russian Academy of Sciences,
Ulyanovsk, Russia
[4] Université Jean Monnet Saint-Etienne, CNRS, Institut d'optique Graduate School,
Laboratoire Hubert Curien UMR 5516, Saint-Etienne, France

e-mail: panyaev.ivan@rambler.ru

Received December 09, 2024
Revised May 06, 2025
Accepted June 14, 2025

The magneto-optical Faraday effect in one-dimensional triply periodic photonic-crystalline structures based on dielectrics (SiO_2, TiO_2) and ferrite garnets (YIG, Bi:YIG) forming supercells of type $[(ab)^N(cd)^M]$was theoretically investigated. The polar magneto-optical configuration, in which the magnetization vectors of the magnetic layers of the photonic crystals are orthogonal to the layer interfaces, and an electromagnetic wave propagating in the photonic-crystal structure has a wave vector component along the direction of the magnetization vectors, was considered. Using the transfer-matrix method, (4×4) frequency-angular spectra of transmission of plane electromagnetic waves through these photonic crystals were obtained. The position and structure of transmission bands in the forbidden photonic zones' spectra, as well as the dependencies of the Faraday rotation angles on frequency and angle of incidence of the electromagnetic wave, were studied for photonic crystals at $N = 3$, $M = 5$ and $K = 7$ (optimal number of periods) and various thicknesses of magnetic layers. It was shown that triply periodic photonic crystals can simultaneously exhibit high transmission coefficients and large Faraday rotation angles, making these structures promising for various technical applications.

Keywords: magneto-optical Faraday effect, photonic bandgap, photonic crystals.

DOI: 10.61011/EOS.2025.08.62024.7412-25

1. Introduction

The magneto-optical Faraday effect is known as the change in the polarization state of an electromagnetic wave (EMW) when passing through a magnetic medium or a complex structure based on magnetic materials. In particular, a manifestation of this effect is the rotation of the polarization plane of a linearly polarized optical beam — the Faraday rotation (FR) [1,2]. Currently, the Faraday effect is widely used to investigate the magnetic structure of thin magnetic films and multilayer magnetic materials [1–3], as well as for various applications, including the creation of nonreciprocal devices such as optical isolators, circulators, or phase shifters [1], magnetic sensors [4], and even chemical detection sensors [5]. Great interest in studying FR stems from the prospects of numerous applications related to the possibility of controlling the effect by external stimuli (external magnetic or electric fields, temperature, etc.) in various functional materials, particularly electro-optical [6,7], plasmonic, magneto-plasmonic structures [8], combined magnetic and electro-optical heterostructures [9], as well as magneto-photonic [10,11] and photonic-magnonic crystals [12–16].

Photonic crystals (PCs), due to their artificially periodic refractive index, have photonic bandgaps (PBGs) in their transmission spectra [17] Breaking the periodicity of the PC by introducing single defect layers or periodically distributed other structural elements leads to the appearance of narrow transmission peaks (defect modes) or sets of peaks — transmission bands of the structure, whose complexity depends on the defect layers architecture. Within the PBG of a single-period PC with a single defect layer, one or several (depending on the defect thickness) narrow transmission peaks can be located. For example, in [18], the half-width of the transmission peak for a PC with a magnetic defect is approximately 1 THz·rad with the PBG width of 0.33 PHz·rad. The presence of defect modes makes it possible to use such PCs as narrowband frequency filters and sensors. Particular interest is focused on PCs with complex elementary cell structures based on several different materials, which form periodic subsystems inside them, due to the modified structure of their PBGs. These include, in particular, two-periodic [12–16] and three-periodic PCs [19–23]. Unlike single-period structures with a defect layer, in more complex systems such as two- and three-periodic PCs, there exist significantly wide transmission bands inside the PBG, which can consist of several closely spaced peaks (analogous to „optical combs“) [12–14]. The number of intra-band transmission bands, their location inside the PBG, and width critically depend on the combination of materials

forming the subcells of the three-periodic PC and the system geometric parameters [19–23]. Incorporating magnetic layers into the structure with a complex elementary cell allows combining the features of a complex three-periodic PC with magneto-optical properties, enabling active control of the optical characteristics of such a system.

In [12], the Faraday effect was studied in photonic-magnonic structures representing one-dimensional two-periodic magnetic PCs based on alternating layers SiO_2, TiO_2 with periodically embedded magnetic layers of yttrium-iron garnet (YIG) $Y_3Fe_5O_{12}$. As is known, YIG, which features low absorption in the near-infrared (IR) range combined with the Faraday effect, is one of the traditional magnetic materials for microwave and magneto-optical applications. However, for miniaturized devices, achieving large polarization plane rotation angles and high detection sensitivity based on FR is a critical and challenging task. To this end, it is necessary to select and search for materials with large FR, such as Ce:YIG [24,25] or Bi:YIG [26], and structures [27] that enhance the Faraday effect. For example, in experiments [28,29] on magnetophotonic structures based on silicon oxide and titanium oxide layers SiO_2, TiO_2 with a complex magneto-optical defect composed of bismuth-substituted yttrium iron garnet Bi:YIG layers, the Faraday rotation reached maximum values of about 20.6°. Thus, to achieve large FR values, an important task is the search for magnetophotonic composites where large FR can be expected for modes localized in the magnetic subsystem [8,11,29–32]. As such media, magnonic-photonic crystals were considered theoretically in [12], where maximum FR values near the intra-band transmission peaks reached approximately 2° (or $0.11°/\mu$m) for s-polarized light and were an order of magnitude less for p-polarized light. It was shown that the positions of FR maxima do not coincide with the frequencies of transmission peaks. Consequently, in magnonic-photonic PCs with transmission near unity, FR angles were of the order of tenths or even hundredths of a degree.

The advantage of the three-periodic structure compared to photonic-crystalline structures with defects, two-periodic PCs, and other conditionally simpler structures lies in a larger number of degrees of freedom to create systems with predetermined optical properties, allowing finer tuning of the PBG center position, regulation of its width, and the position and sharpness of PBG edges [19–23].

The present work aims to find such PC systems in which the maxima of FR and high transmission coefficients of EMW are spectrally coincident. To this end, a more complex structure — a three-periodic magnetic PC — is considered, based on layers of four different materials a, b, c, d, whose elementary cell $[(ab)^N(cd)^M]$ is composed of fragments of two different PCs $(ab)^N$ and $(cd)^M$, where N, M is the number of corresponding periods. The subcells of the three-periodic PC (ab) and (cd) can be formed from layers a, b, c and d in many different ways, and, as shown in [19], the optical properties of such PCs can differ significantly depending on the choice of materials and layer alternation. Differences are manifested in transmission (reflection) spectra — in the position and width of the PBG, the number and location of intra-band transmission (reflection) bands, and their structure. In [33], a three-periodic magnetic PC was considered, in which the first cell (ab) consisted of nonmagnetic dielectric layers SiO_2 and TiO_2, and the second (cd) — of magnetic bigyrotropic layers YIG and Bi:YIG. This material choice allowed obtaining a significantly wide PBG with a set of narrow intra-band transmission peaks [33]. In this work, attention is focused on a three-period PC in which both constituting subcells contain magnetic layers YIG or Bi:YIG, resulting in a PBG and transmission bands structure distinct from previous ones.

2. Description of the system and Theory

Let us consider a three-periodic PC $[(SiO_2/YIG)^N(TiO_2/Bi{:}YIG)^M]^K$, whose supercell, repeated K times, represents a combination of fragments of two magnetic periodic structures $(SiO_2/YIG)N$ and $(TiO_2/Bi{:}YIG)M$ (Fig. 1, a). Hereafter, for simplicity of notation, we introduce the following symbols for layers SiO_2, TiO_2, YIG and Bi:YIG:S, T, Y, B respectively. Thus, the PC structure is designed as $[(SY)^N(TB)^M]^K$. The thicknesses of the subcells (SY) and (TB), i.e., the subperiods, are designated as $D_1 = d_S + d_Y$ and $D_2 = d_T + d_B$, and the thickness of the supercell (superperiod) is $D_3 = ND_1 + MD_2$. The total thickness of the considered structure consisting of K superperiods is equal to KD_3. The layers of the PC are arranged parallel to the (xy) plane, and the z axis coincides with the growth axis of the PC. It is assumed that the longitudinal dimensions of the PC along the x and y axes are large enough so that boundary effects in these directions can be neglected.

The YIG and Bi:YIG layers are magnetized to saturation along or opposite to the z axis by applying an external magnetic field $\mathbf{H}_0$ in the corresponding direction. Taking into account first-order small terms in components of the magnetization vector, the tensors of dielectric permittivity and magnetic permeability have the following form [1]:

$$\hat{\varepsilon}_j = \begin{pmatrix} \varepsilon_j & i\varepsilon'_j & 0 \\ -i\varepsilon'_j & \varepsilon_j & 0 \\ 0 & 0 & \varepsilon_j \end{pmatrix},$$

$$\hat{\mu}_i = \begin{pmatrix} \mu_i & i\mu' & 0 \\ -i\mu_j & \mu_j & 0 \\ 0 & 0 & \mu_j \end{pmatrix}, \ (j = Y, B), \qquad (1)$$

where the magnetization-induced off-diagonal elements ε_j and μ_j are responsible for the bigyrotropic properties of the ferrite garnets YIG and Bi:YIG. The nonmagnetic dielectrics SiO_2 and TiO_2 possess isotropic optical properties and are characterized by the corresponding diagonal tensors $\varepsilon_{S(\alpha\beta)} = \varepsilon_S\delta_{\alpha\beta}$, $\mu_{S(\alpha\beta)} = \delta_{\alpha\beta}$, $\varepsilon_{S(\alpha\beta)} = \varepsilon_T\delta_{\alpha\beta}$, $\mu_{T(\alpha\beta)} = \delta_{\alpha\beta}$ ($\alpha\beta = x, y, z$; with$\delta_{\alpha\beta}$ — being the Kronecker delta symbol

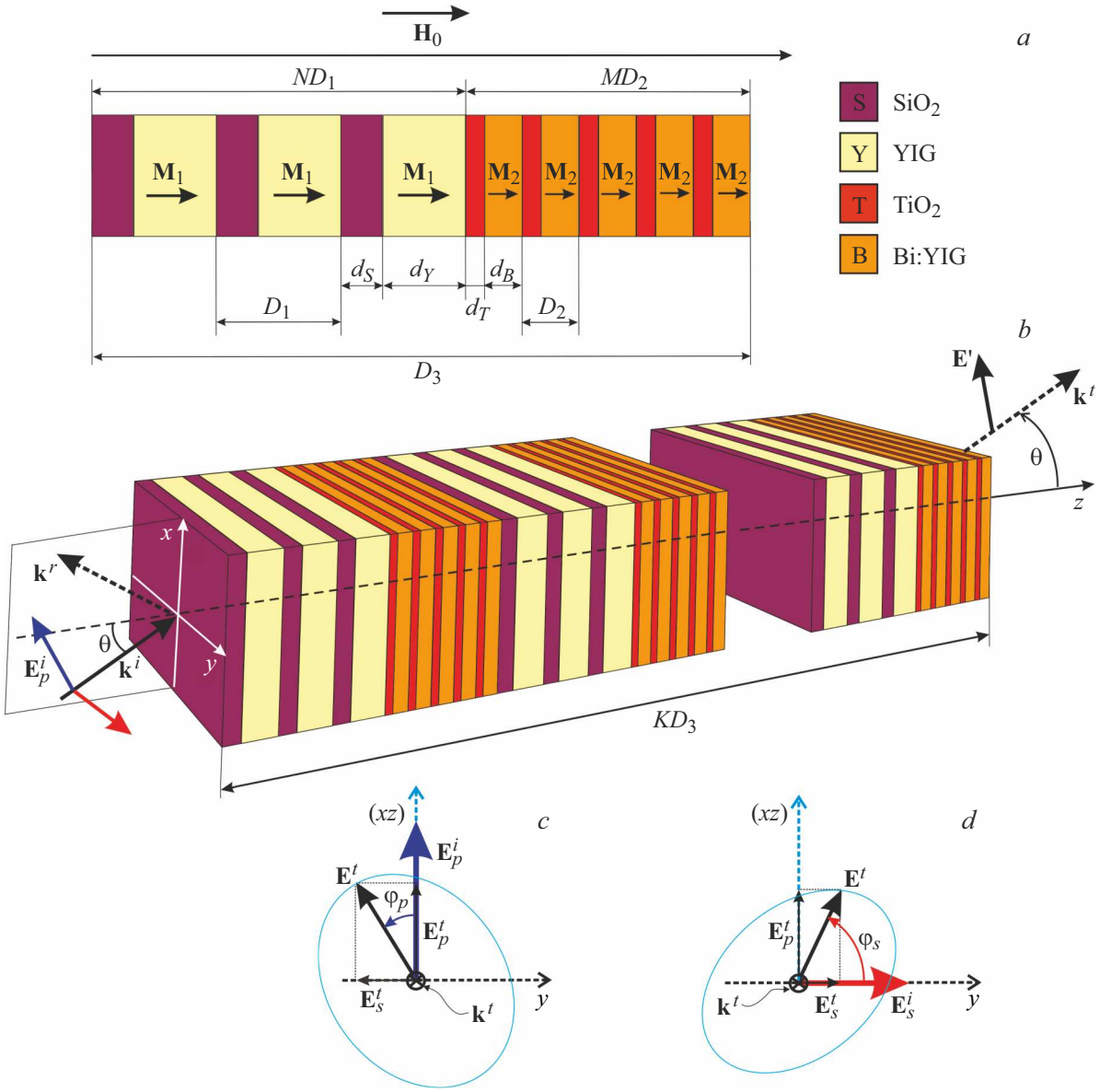

Figure 1. The schematic of the three-periodic magneto-optical photonic crystal $[(SY)^N(TB)^M]^K$: *a* — photonic crystal supercell at $N = 3$, $M = 5$ (black arrows indicate the magnetization vectors $\mathbf{M}_1$ and $\mathbf{M}_2$ in the YIG and Bi:YIG layers, respectively), $\mathbf{H}_0$ — is constant external magnetic field. *b* — is the Faraday effect when an EMW passes through the three-periodic photonic crystal. Blue and red arrows indicate the electric components of the incident EMWs with *s*- or *p*-polarizations ($\mathbf{E}_s^i$, $\mathbf{E}_p^i$ respectively), and the black arrow shows the electric field vector of the transmitted EMW $\mathbf{E}^t$. *c* and *d* are schematic representations of the Faraday rotation angles φ_p and φ_s for the cases of incident EMWs with *p* and*s*-polarizations, respectively. Vertical dashed lines show the projection of the plane (xz).

All materials forming the PC structure are transparent in the near-infrared wavelength range and have real dielectric permittivity values ε_j $(j = 0, S, T, Y, B)$, with the input and output media (air) designated as 0.

A plane electromagnetic wave of *s*- or *p*-polarization (red $(\mathbf{E}_s^i)$ or blue $(\mathbf{E}_p^i)$ vectors in Fig. 1, *b*), with angular frequency ω and wave vector $\mathbf{k}_0^i = (k_x, 0, k_{0z})$ is incident from air onto the PC surface at an angle θ such that the plane of incidence is the (xz) plane. Considering the direction of magnetization vectors in the YIG and Bi:YIG layers, this corresponds to the polar magneto-optical (MO) configuration [1] used in Fig. 1, *b*. In this case, the normal EMWs in the magnetic media are waves with elliptical polarizations $\mathbf{k}_{zj}^{\pm} = (k_x 0, k_{zj}^{\pm})$, $(j = Y, B)$:

$$k_{zj}^{\pm} = \Big(\Omega^2(\varepsilon_j\mu_j + \varepsilon_j'\mu_j') - k_x^2 \pm \Omega(\varepsilon_j\mu_j' + \mu_j\varepsilon_j') \times \left[(-k_x^2 + \Omega^2\varepsilon_j\mu_{kj})/\varepsilon_j\mu_j\right]^{1/2}\Big)^{1/2}, \quad (2)$$

where notation $\omega = \omega/c$ is introduced.

The transmitted EMW $\mathbf{E}^t$ is elliptically polarized, with its polarization plane rotated by angle φ_s or φ_p (the FR angle)

relative to the polarization plane of the incident wave of s- or p-polarization, respectively (Fig. 1, c and d).

The electric and magnetic fields in bigyrotropic layers can be written as superpositions of four waves: two (incident) waves propagating along the $\mathbf{z}$ axis and two waves propagating in the opposite direction (reflected), denoted by indices i and r:

$$E_{\alpha,j}(z) = E^{i+}_{\alpha,j}\exp(lk^{+}_{z\,j}z) + E^{r+}_{\alpha,j}\exp(-ik^{+}_{z\,j}z) + E^{i-}_{\alpha,j}\exp(ik^{-}_{z\,j}z) + E^{r-}_{\alpha,j}\exp(-ik^{-}_{z\,j}z),$$

$$H_{\alpha,j}(z) = E^{i+}_{\alpha,j}\exp(lk^{+}_{z\,j}z) + H^{r+}_{\alpha,j}\exp(-ik^{+}_{z\,j}z) + H^{i-}_{\alpha,j}\exp(ik^{-}_{z\,j}z) + H^{r-}_{\alpha,j}\exp(-ik^{-}_{z\,j}z), \quad (3)$$

where $\alpha = x, y, z,\ j = Y, B$.

In each of the isotropic layers SiO_2 and TiO_2 the electromagnetic radiation is a superposition of independent s- and p-polarized waves with components of wave fields $\{H_x, E_y, H_z\}$ and $\{E_x, H_y, E_z\}$ respectively, with wave vectors $\mathbf{k}_j = (k_x, 0, k_{jz})$, $(j = S, T)$ coinciding:

$$E_{\alpha,j}(z) = E^{i}_{\alpha,j}\exp(ik_q z) + E^{r}_{\alpha,j}\exp(-ik_q z),$$

$$H_{\alpha,j}(z) = H^{i}_{\alpha,j}\exp(ik_q z) + H^{r}_{\alpha,j}\exp(-ik_q z). \quad (4)$$

Here $k_q = \sqrt{-k_x^2 + \Omega^2\varepsilon_j\mu_j}$ — z-components of wave vectors, coinciding for s- and p-polarized waves in each isotropic medium.

From Maxwell's equations supplemented by material relations for bigyrotropic media, relations between amplitudes of components of electric and magnetic fields are obtained:

$$H_x^+ = -\delta_\varepsilon^+ E_y^+,\ E_x^+ = i\gamma_s^+ E_y^+,\ H_y^+ = -i\beta_\varepsilon^+ E_y^+,$$

$$E_x^- = \delta_\mu^- H_y^-,\ H_x^- = i\gamma_\mu^- H_y^-,\ E_y^- = -i\beta_\mu^- H_y^-, \quad (5)$$

where coefficients $\beta^+_{\varepsilon j}$, $\gamma^+_{\varepsilon j}$ and $\delta^+_{\varepsilon j}$ are defined as

$$\gamma^+_{\varepsilon j} = i\left[\varepsilon'_j(\varepsilon_j\Delta\mu_j\Omega^2 - \mu_j k_x^2) + \mu'_j\varepsilon_j(k^+_{z\,j})^2\right]/N_{\varepsilon j}(k^+_{z\,j}),$$

$$\delta^+_{\varepsilon j} = k_q^+\varepsilon_J\left[(k^+_{z\,j})^2 - k_x^2 - \Omega^2(\varepsilon_j\mu_j + \varepsilon'_j\mu'_j)\right]/N_{\varepsilon j}(k^+_{z\,j}),$$

$$\beta^+_{\varepsilon j} = i\varepsilon_j\mu'_j + \mu_j\varepsilon'_j)k^+_{z\,j}\Omega/N_{\varepsilon j}(k^+_{z\,j}) \quad (6)$$

and the following notations are introduced

$$N_{\varepsilon j}(k^+_{z\,j}) = \varepsilon\mu[(k^+_{z\,j})^2 + k_x^2] - \Omega^2\varepsilon^2\Delta\mu,$$

$$\Delta\varepsilon_j = \varepsilon_j^2 - \varepsilon'^2_j,\ \delta\mu_j = \mu_j^2 = \mu'^2_j - \mu'^2_j.$$

Other coefficients $\beta^+_{\mu j}, \gamma^+_{\mu j}$ and $\delta^+_{\mu j}$ are obtained from corresponding expressions (6) by replacing $\varepsilon \leftrightarrow \mu$.

To find the amplitudes of the transmitted EM wave, the standard transfer matrix method of dimension (4×4) is used [34]. To express continuity equations for tangential components of electric $E_{x,y}$ and magnetic $H_{x,y}$ fields at each interface of media, we introduce column vectors of field amplitudes in each PC layer:

$$\boldsymbol{\psi}_j = (E^{I+}_{yj}\, E^{r+}_{yj}\, H^{I-}_{yj}\, H^{r-}_{yj})^\tau,$$

where τ denotes the transpose operation. Similarly, for the input and output media (taking into account the presence of reflected wave in the former and transmitted wave in the latter), one can write:

$$\boldsymbol{\psi}_0^{\text{in}} = (E^{I(s)}_{y0}\, E^{r(s)}_{y0}\, H^{I(p)}_{y0}\, H^{r(p)}_{y0})^\tau,$$

$$\boldsymbol{\psi}_0^{\text{out}} = (E^{t(s)}_{y0}\, 0\, H^{t(p)}_{y0}\, 0)^\tau.$$

The photonic crystal of type $[(SY)^N(TB)^M]^K$ contains $2K(N+M)+1$ interfaces between media, including external boundaries with air, each governed by 4 algebraic equations. From this system of $4[2K(N+M)+1]$ equations, successively eliminating field amplitudes inside the PC, we arrive at a system of four algebraic equations connecting fields in air at opposite boundaries of the PC, written in matrix form as:

$$\hat{A}_0\hat{E}_0(KD_3)\boldsymbol{\psi}_0^{(\text{out})} = \hat{A}_S(\hat{T}_g)^K\hat{S}_{S0}\boldsymbol{\psi}_0^{(\text{in})}. \quad (7)$$

Here, $\hat{A}_S(\hat{T}_g)^K\hat{S}_{S0}$ is the transfer matrix of dimension (4×4) linking field amplitudes of waves at points $z = 0$ and $z = KD_3$ at the left-hand sides of the external surfaces of the PC. Here, $\hat{T}_g = \hat{S}_{SB}(\hat{T}_{02})^M\hat{S}_{BS}|(\hat{T}_{01})^N$ is the transfer matrix for the supercell, and $\hat{T}_{01}$ and $\hat{T}_{02}$ are transfer matrices for subcells (SY) and (BT) respectively:

$$\hat{T}_{01} = \hat{S}_{SY}\hat{E}_Y(d_T)\hat{S}_{YS}\hat{E}_S(d_S),$$

$$\hat{T}_{02} = \hat{S}_{BT}\hat{E}_T(d_T)\hat{S}_{TS}\hat{E}_B(d_B). \quad (8)$$

Matrices $\hat{S}_{ij} = \hat{A}_i^{-1}\hat{A}_j$ and $\hat{S}_{S0} = \hat{A}_S^{-1}\hat{A}_0$ connect field amplitudes across the boundary of layers i and j respectively, as well as at the boundary of layer S and air:

$$\boldsymbol{\psi}_i = \hat{S}_{ij}\boldsymbol{\psi}_j,$$

$$\boldsymbol{\psi}_S = \hat{S}_{S0}\boldsymbol{\psi}_0^{\text{in}}. \quad (9)$$

Coefficient matrices $\hat{A}_j$ used to compute matrices $\hat{S}_{ij}$ in expressions (9) for magnetic layers $(j = Y, B)$ have the following form:

$$\hat{A}_j = \begin{pmatrix} 1 & 1 & \eta^-_{\mu j} & -\beta^-_{\mu j} \\ \delta^+_{\varepsilon j} & -\delta^+_{\varepsilon j} & \gamma^-_{\mu j} & \gamma^-_{\mu j} \\ -\beta^+_{\varepsilon j} & \beta^+_{\varepsilon j} & 1 & \\ \gamma^+_{\varepsilon j} & \gamma^+_{\varepsilon j} & -\delta^-_{\mu j} & \delta^-_{\mu j} \end{pmatrix}. \quad (10)$$

For nonmagnetic layers of the PC $(j = S, T)$ and for air $(j = 0)$ the matrices $\hat{A}_j$ have quasi-diagonal form:

$$\hat{A} = \begin{pmatrix} \hat{A}_j^{(s)} & \hat{0} \\ \hat{0} & \hat{A}_j^{(p)} \end{pmatrix},$$

where matrices $\hat{A}_j^{(s)}$ and $\hat{A}_j^{(p)}$ are matrices of dimension (2×2) for s- and p-polarized waves:

$$\hat{A}_j^{(s)} = \begin{pmatrix} 1 & 1 \\ \delta^+_{\varepsilon j} & -\delta^+_{\varepsilon j} \end{pmatrix},\quad \hat{A}_j^{(p)} = \begin{pmatrix} 1 & 1 \\ -\delta^-_{\mu j} & \delta^-_{\mu j} \end{pmatrix},$$

$$\delta_{\varepsilon j}^{+} = k_{z\,j}/\Omega\varepsilon_j, \quad \delta_{\mu j}^{-} = k_{z\,j}/\Omega\mu_j,$$

and $\hat{0}$ are zero matrices of dimension (2×2).

Diagonal matrices $\hat{E}_j(d_j)$ in equations (7):

$$\hat{E}_j(d_j) = \Big(\exp(ik_{z\,j}^{+}d_j)\exp(-ik_{z\,j}^{+}d_j)\exp(ik_{z\,j}^{-}d_j) \times \exp(-ik_{z\,j}^{-}d_j)\Big), \quad (j = Y, B),$$

$$\hat{E}_j(d_j) = \Big(\exp(ik_{z\,j}d_j)\exp(-ik_{z\,j}d_j)\exp(ik_{z\,j}d_j) \times \exp(-ik_{z\,j}^{-}d_j)\Big), \quad (j = S, T)$$

characterize the phase progression inside the layers j, and $\hat{E}_0(k_{z0}KD_3)$ is defined as

$$\hat{E}_0(k_{z0}KD_3) = \Big(\exp(ik_{z0}KD_3)\exp(-ik_{z0}KD_3) \times \exp(ik_{z0}KD_3)\exp(-ik_{z0}^{-}KD_3)\Big).$$

The system of equations (7) allows finding the relation between the amplitudes of the incident and the transmitted waves via the amplitude transmission coefficients T_{ss}, T_{pp}, T_{sp} and T_{ps}, which are complex functions of frequency and EMW incidence angle:

$$\begin{pmatrix} E_s^{(t)} \\ E_p^{(t)} \end{pmatrix} = \begin{pmatrix} T_{ss} & T_{sp} \\ T_{ps} & T_{pp} \end{pmatrix} \begin{pmatrix} E_s^{(i)} \\ E_p^{(i)} \end{pmatrix}. \qquad (11)$$

When the incident electromagnetic radiation contains only s-polarized component ($\mathbf{E}_p^i = 0$) or only p-polarized component ($\mathbf{E}_s^i = 0$), the energy transmission coefficients, defined as ratios of transmitted to incident intensity, can be written as:

$$T_s = |T_{ss}|^2 + |T_{ps}|^2 \ (\text{at } \mathbf{E}_p^i = 0),$$

$$T_p = |T_{sp}|^2 + |T_{pp}|^2 \ (\text{at } \mathbf{E}_s^i = 0). \qquad (12)$$

Note that in the absence of absorption, energy reflection coefficients are determined by:

$$R_s = 1 - T_s, \quad R_p = 1 - T_p.$$

Faraday rotation angles φ_s and φ_p for incidence of s- or p-polarized waves on the PC surface are defined as in the monograph [2]:

$$\tan\varphi_s = -\mathrm{Re}\Big(\frac{T_{ps}}{T_{ss}}\Big), \ \tan\varphi_p = \mathrm{Re}\Big(\frac{T_{sp}}{T_{pp}}\Big). \qquad (13)$$

3. Numerical Calculations and Discussion

For numerical calculations of transmission coefficients and FR angles upon transmission of the EMW through the studied PC, we consider the frequency dispersion of refractive indices $n_j(\omega)$ of the materials in the near-infrared range according to [35–39]. For nonmagnetic materials SiO_2, TiO_2 the dielectric permittivity is given by $\varphi_j(\omega) = (n_j(\omega))^2$, $(j = S, T)$ [35,36]. For YIG, the dispersion dependence of the diagonal elements of the dielectric permittivity tensor $\varepsilon_Y(\omega)$ is defined as in [37], the diagonal elements of the magnetic permeability tensor are $\mu_Y = 1$, whereas the off-diagonal tensor elements are equal to $\varepsilon_Y' = -2.47 \cdot 10^{-4}$, $\mu_T' = 8.76 \cdot 10^{-5}$respectively [38]. For Bi:YIG, the corresponding material parameters have the following values $\varepsilon_B = 5.76$ [39,40], $\mu_B = 1$, $\mu_B' = 1.65 \cdot 10^{-5}$ [41,42].

The thicknesses of the layers in the subcells (SY) and (TB) d_{0j} were chosen according to the Bragg condition [43]:

$$n_j(\lambda_{01,2})d_{0j} = \lambda_{01,2}/4, \qquad (14)$$

where $\lambda_{01,2}$ are the Bragg wavelengths of the subcells (SY) and (TB) respectively, and $n_j(\lambda_{01,2})$ are the refractive indices of the layers at the corresponding Bragg wavelength. We estimate the characteristic size of the PC structure by taking the Bragg wavelengths of the subcells equal to the main telecommunication wavelength, i.e., $\lambda_{01} = \lambda_{02} = 1.55\,\mu$m. Taking into account the dispersion of the refractive indices at this wavelength, we obtain the following layer thicknesses: $d_{0S} = 0.269\,\mu$m, $d_{0T} = 0.158\,\mu$m, $d_{0Y} = 0.176\,\mu$m, $d_{0B} = 0.162\,\mu$m. Thus, the thickness of the structure$[(SY)^3(TB)^5]^7$ is equal to $20.545\,\mu$m.

From a practical point of view, the most interesting frequency range corresponds to the telecommunications wavelengths $\lambda_0 = 1.55\,\mu$m $(\omega_0 \approx 1.215\,\text{rad·PHz})$ and $\lambda_0 = 1.3\,\mu$m $(\omega_0 \approx 1.449\,\text{rad·PHz})$. Figures 2, *a, b* show the frequency-angle dependencies of the energy transmission coefficients $T_s(\omega, \theta)$ and$T_p(\omega, \theta)$ in the region of the first PBG for s and p-polarized incident EMWs for the PC structure $[(SY)^3(BT)^5]^7$. Figures 2, *c, d* and *e, f* show detailed fragments of the intraband transmission bands for EMWs of s and p-polarizations; vertical lines in Figs. 2 *c, d* correspond to the frequency $\omega_0 \approx 1.215\,\text{rad·PHz}$ $(\lambda_0 = 1.55\,\mu\text{m})$, and in Figs. 2, *e, f* — $\omega_0 \approx 1.449\,\text{rad·PHz}$.

As seen in Figs. 2, *a, b*, both PBGs contain four significantly broad internal transmission bands, whose half-widths at $\theta = 0$ are $\Delta\omega_1 \approx 0.078\,\text{PHz·rad}$, $\Delta\omega_2 \approx 0.056\,\text{PHz·rad}$, $\Delta\omega_3 \approx 0.106\,\text{PHz·rad}$ and $\Delta\omega_4 \approx 0.077\,\text{PHz·rad}$. For comparison, in the two-periodic magnetophotonic crystal $[\text{YIG}/(\text{TiO}_2/\text{SiO}_2)^4/\text{TiO}_2]^5$ [13] the corresponding values are of about 0.01 PHz·rad, i.e., roughly 5−10 times narrower than in the case of the three-periodic PC.

Each transmission band (Fig. 2, *c–f*) has a complex structure split into six peaks, where the transmission coefficient reaches values close to unity. This multiplicity of splitting, as shown in works [13,14], is determined by the number of superperiods of the structure and equals $(K - 1)$, which in the present case (with $K = 7$) gives six maxima. In certain parts of the transmission bands, these peaks can merge into a „plateau," where the transmission coefficient slightly fluctuates, not reaching unity (e.g., Fig. 2, *e*).

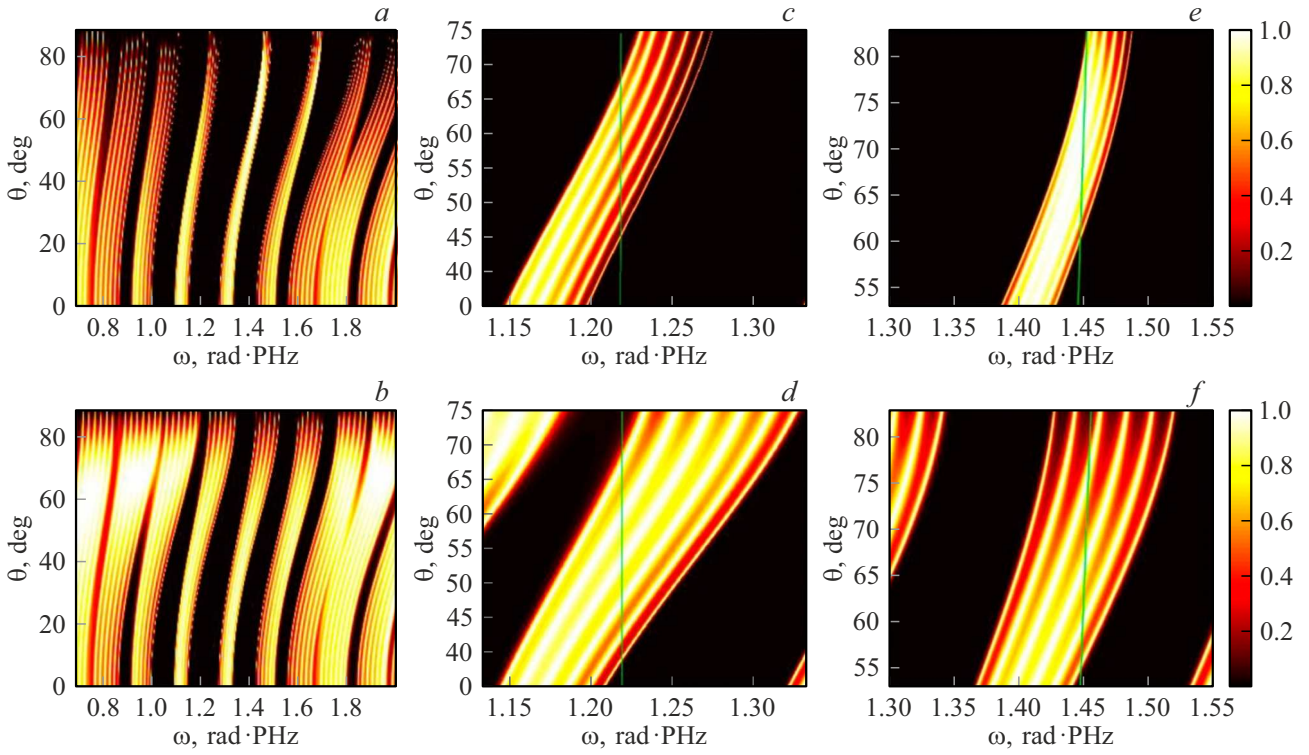

Figure 2. Transmission spectra of $T_s(\omega, \theta)$ and $T_p(\omega, \theta)$ for the cases of s and p-polarized incident EMWs (upper and lower lines, respectively) for FC $[(SY)^3(TB)^5]^7$: a, b — in the first ZFZ; c, d a fragment of the intraband transmission band near $\lambda_0 = 1.55\,\mu$m ($\omega_0 \approx 1.215$ rad·PHz); e, f — near $\lambda_0 = 1.3\,\mu$m ($\omega_0 \approx 1.449$ rad·PHz). The Bragg wavelengths for both cells is equal to $\lambda_{01} = \lambda_{02} = 1.55\,\mu$m. Vertical green lines in Fig. c–f mark the frequencies $\omega_0 \approx 1.215$ rad·PHz and $\omega_0 \approx 1.449$ rad·PHz. The color scale represents values of T_s, T_p.

At a fixed frequency, increasing the incidence angle causes the peaks to become less pronounced: the difference between the adjacent maxima and minima of the transmission coefficient within the intraband transmission band decreases. At a fixed incidence angle θ increasing EMW frequency increases the contrast of transmission peaks, especially for s-polarized waves (Figs. 2, c, e).

At normal incidence ($\theta = 0$) positions of the PBG edges and of the intraband transmission bands practically coincide. With deviation of the incidence angle from normal, the PBG of s-polarized waves broadens, whereas that of p-polarized waves narrows. Meanwhile, the behavior of transmission bands with increasing θ is inverse: the intraband transmission bands of s-polarized waves noticeably narrow, whereas those of p-polarized waves expand (Figs. 2, *a, b*).

Besides the intraband transmission modes, a characteristic feature of transmission spectra of three-periodic structures is the presence of satellite zones at edges of the main PBG, which can open with increasing θ for example, the satellite zone for s-polarized waves is located below 0.8 rad·PHz at angles $\theta > 40°$, and for p-polarized waves at$\theta > 75°$ to the right of the high-frequency edge of the main PBG. Furthermore, in the spectrum of p-polarized waves, the low-frequency edge of the PBG can merge with the intraband transmission band, as in Fig., b at $\theta > 55°$. Finally, increasing θ causes a blue shift of the spectrum, which is characteristic of all 1D PC structures.

It should be noted that in a PC of type $[(SY)^3(BT)^5]^7$ intraband transmission bands are significantly broader than in the PC$[(ST)^3(YB)^{10}]^3$, considered in our previous work [33]. For example, for $[(SY)^3(BT)^5]^7$ at $\lambda_0 = 1.55\,\mu$m and $\theta = 54°$ the width of the second intraband transmission band (located near $\theta = 0$ in the interval1.0 rad·PHz $< \omega <$ 1.2 rad·PHz Fig. 2)) is $\Delta\omega_s = 0.052$ rad·PHz for s-polarized EMWs and $\Delta\omega_p = 0.083$ rad·PHz for p-polarized wave whereas the corresponding values for structure $[(ST)^3(YB)^{10}]^3$ are $\Delta\omega_s = 0.011$ rad·PHz and $\Delta\omega_p = 0.023$ rad·PHz.

Figures 3, *a, b* show dependencies of the transmission coefficients and FR angles for the structure $[(SY)^3(BT)^5]^7$ on the EMW incidence angle at the selected wavelength $\lambda_0 = 1.55\,\mu$m for s and p-polarized waves respectively. Similarly, angular dependencies T_s and T_p at $\lambda_0 = 1.3\,\mu$m are presented in Figs. 3, c, d. Red and blue curves correspond to the transmission coefficients, green and orange correspond to the FR angles, calculated using formula (13). Each of the six maxima of the transmission coefficients $T_{s(\max)}$ and $T_{p(\max)}$ has values close to 1 at the angles $\theta_{s\alpha}$ and $\theta_{p\alpha}|$, respectively ($\alpha = 1, \ldots, 6$), and the minimum values between the peaks in the transmission band are far from zero: not less than $T_{s(\min)} = 0.18$ and $T_{p(\min)} = 0.25$ for

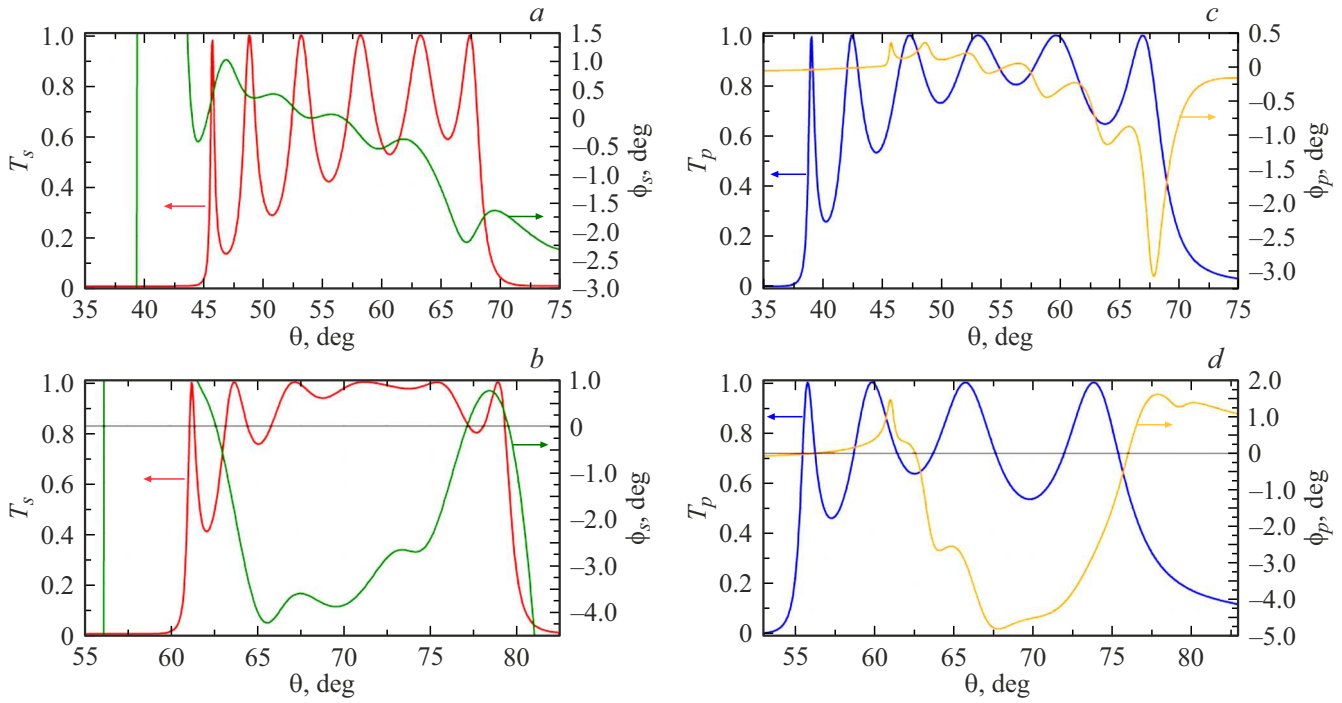

Figure 3. Angular dependencies of the transmission coefficients and FR angles: a, c — $T_s(\theta)$ and $\varphi_s(\theta)$; b, d — $T_p(\theta)$ and $\varphi_p(\theta)$ for the structure $[(SY)^3(TB)^5]^7$ at $\lambda = 1.55\,\mu$m (a, b), $\lambda = 1.3\,\mu$m (c, d). The red and blue curves correspond to the transmission coefficients, while the green and orange curves correspond to the FR angles.

s and p-polarized waves at$\lambda_0 = 1.55\,\mu$m (Fig. 3, *a, b*) and similarly $T_{s(\min)} = 0.4$ and $T_{p(\min)} = 0.45$ at $\lambda_0 = 1.3\,\mu$m (Fig. 3, *a, b*).

As can be seen from comparison of Figs. 3, *a* and *b*, and Figs. 3, *c* and *d*, the angular transmission region ofs-polarized EMWs is somewhat narrower than that of *p*-polarized ones, and its left edge T_s is shifted towards larger θ angles compared to the left edge T_p: the positions of the first transmission peaks correspond to incidence angles $\theta_{s1} = 45.80°$ and $\theta_{p1} = 39.13°$ for $\lambda_0 = 1.55\,\mu$m (Fig. 3, *a, b*). The positions of the last (sixth) transmission peaks for waves of both polarizations differ much less: $\theta_{s6} = 67.4°$ and $\theta_{p6} = 66.93°$. For *s*-polarized waves, the angular distance between the extreme transmission peaks is $\Delta\theta_s = 21.6°$ whereas for *p*-polarized EMWs, $\Delta\theta_p = 27.8°$. As for FR angles, they vary within $3.05° \le \varphi_p \le 0.3°$ and $-2.3° \le \varphi_s \le 1.0°$ in the transmission band. At the negative maximum FR value, the EMW transmission coefficient is high: $T_s = 0.9$, but at the positive maximum of the FR it is only $T_s = 0.15$ at the incidence angle $\theta_s \approx 44°$. Here onward, $\varphi^{\pm}_{s(\max)}$ denote the maximal positive or negative FR for the given parameters. For *p*-polarized waves, $\varphi^{-}_{p(\max)} = -3.05°$ at $\theta_s \approx 66°$ also coincides with good EMW transmission: $T_p = 0.82$, while $\varphi^{+}_{p(\max)} = 0.3°$ correspond to transmission coefficients $T_p = 0.65$ and $T_p = 0.85$ at $\theta_p \approx 46°$ and $\theta_p \approx 48°$ respectively.

It is also worth noting that in some frequency intervals and at certain incidence angle ranges, FR angles can reach several tens of degrees, for example at $39° \le \theta \le 43°$ for *s*-polarized EMWs (Figs. 3, *a, b*). However, these regions correspond to absence of the transmission ($T_s \to 0$), which is of no practical importance.

For $\lambda_0 = 1.3\,\mu$m maximum Faraday rotation angles are even somewhat larger: $\varphi^{-}_{s(\max)} = -4.2°$ at $T_s = 0.79$ and $\varphi^{-}_{p(\max)} = -4.78°$ at $T_p = 0.71$ (compare Figs. 3, *a, b* and *c, d*).

Next, let us consider frequency dependencies of the transmission coefficients and the FR angles at the incidence angles$\theta_{s\alpha}$ and $\theta_{p\alpha}$ defined above and corresponding to transmission peaks at $\lambda_0 = 1.55\,\mu$m ($\omega_0 \approx 1.215$ rad·PHz). Figure 4 shows the frequency dependences of the transmission coefficients $T_s(\omega)$ and $T_p(\omega)$ and the FR angles $\varphi_s(\omega)$ and $\varphi_p(\omega)$ for *s* and *p*-polarized EMWs (left and right columns respectively) at the incidence angles$\theta_{s1} = 45.80°$ (a) and $\theta_{p1} = 39.13°$ (d); $\theta_{s6} = 67.40°$ (b); $\theta_{p6} = 66.93°$ (c). These angles correspond to the first and sixth peaks T_s and T_p in Fig. 3, *a, b* respectively. For *s*-polarized waves, within the transmission band, the FR angle values vary within $-4.73° \le \varphi_s \le 0.99°$ at $\theta_{s1} = 45.80°$ and $-2.16° \le \varphi_s \le 0.59°$ at $\theta_{s6} = 67.40°$. However, the largest in absolute value negative Faraday rotations $\varphi^{-}_{s(\max)} = -4.73°$ occur at low $T_s = 0.067$ and at $\theta_{s1} = 45.80°$. The transmission coefficient maxima close to unity $T_s = 0.99$ (the first, lowest frequency peak at $\omega = 1.166$ rad·PHz), corresponds to $\varphi_s = -2.98°$, and also $\varphi_s = -1.45°$ (the second peak at $\omega = 1.174$ rad·PHz).

For the considered PC structure, positive FR can also occur but is somewhat weaker. At $\theta_{s1} = 45.80°$

positive FR corresponds to a narrow frequency interval $1.202\,\text{rad·PHz} \le 1.216\,\text{rad·PHz}$ in the region of the fifth and sixth transmission peaks (Fig. 3, *a*), while at $\omega = 1.112\,\text{rad·PHz}$ the maximal positive FR $\varphi_s = 0.99°$ is reached with a low transmission coefficient $T_s = 0.134$.

With increasing incidence angle, the frequency range corresponding to positive FR angle φ_s expands, covering at $\theta_{s6} = 67.40°$ intervals from the third to the fifth peaks and the gap between the second and third peaks: $1.226\,\text{rad·PHz} \le \omega \le 1.255\,\text{rad·PHz}$, while shifting upwards in frequency together with the transmission band (Fig. 4, *a, b*). The maximal positive rotation $\varphi^{+}_{s(\max)} = 0.598°$ at $\omega = 1.241\,\text{rad·PHz}$ occurs at $\theta_{s6} = 67.40°$.

For *p*-polarized EMWs, the maximal FR angles correspond to somewhat larger T_p values than for *s* polarization. Unlike the *s* case, the frequency ranges where the FR is positive are very narrow (Fig. 4, *c, d*).

By comparison, in [12] for two-period PCs of the type $[\text{YIG}/(\text{TiO}_2/\text{SiO}_2)^4]^5/\text{YIG}$ theoretical calculations showed that near the intraband transmission peaks the maximum FR angles (up to 0.25° for *p*-polarized light and about 1.8° for *s*-polarized light) correspond to low transmission. At frequencies of the intraband transmission modes, the FR peaks are small: rotation reaches up to 0.1° for the incident *s*-polarized light, whereas for the incident *p*-polarized light it does not exceed −0.02° at the corresponding transmission peaks. The FR values for the three-periodic structure $[(SY)^3(TB)^5]^7$ obtained in the present work can at certain frequencies significantly (by about −two orders of magnitude) exceed the values for magnonic-photonic crystals [12], with the FR maxima φ_s and φ_p overlapping with areas of high transmission.

Thus, at fixed incidence angles, tuning the frequency within the transmission bands allows achieving excellent results — substantial FR angles with maximal EMW transmission.

For even greater enhancement of the Faraday effect in the three-period PC, one can select magneto-optical YIG and Bi:YIG layers of larger thickness d_Y, d_B compared to those used in the previous calculations, while keeping the thicknesses of the nonmagnetic layers d_S and d_T unchanged. Figures 5, *a, b* show the dependencies of transmission coefficients T_s, T_p, and FR angles φ_s, φ_p at the wavelength $\lambda_0 = 1.55\,\mu\text{m}$ at *n*-fold increase of d_Y and d_B.

As seen in Figs. 5, *a, b*, with *n*-fold increase of the thickness of the magnetic layers, the angular transmission regions narrow significantly and shift towards smaller incidence angles. For example, for *s*-polarized waves at $n = 1$ (magnetic layers without thickness increase), the angular distance between extreme (first and sixth) transmission peaks T_s equals $\Delta\theta_s = 21.60°$, $\Delta\theta_s = 11.48°$ at $n = 3$ and $\Delta\theta_s = 9.34°$ at $n = 5$. Corresponding values for $\Delta\theta_p$ *p*-polarized EM waves are somewhat larger and at $n = 1$ at $\Delta\theta_p = 27.87°$ at $n = 3$: $\Delta\theta_p = 14.31°$, while at $n = 5$: $\Delta\theta_p = 10.87°$. Together with peaks T_s and T_p the graphs of the dependences of the FR angles (Fig. 5, *c, d*) also shift, and the values of φ_s and φ_p, falling into the angular transmission region $(0 \le T_{s,p}(\theta) \le 1)$, increase significantly. The maximal negative rotation at $n = 1$ is for *s*–polarized wave $\varphi^{-}_{s(\max)} = -2.19°$ at $\theta_s = 67.07°$ with a transmission coefficient of $T_s = 0.926$. The maximal positive rotation $\varphi^{+}_{s(\max)} = 1.02°$ occurs at $\theta_s = 46.93°$, with a low transmission coefficient: $T_s = 0.129$. At the sixth peak $T_s = 0.998$ $\varphi_s = -2.17°$ is reached. Note that the region of high (up to several tens of degrees) φ_s values does not coincide with the transmission band and is not considered as a potentially applicable result.

For *p*-polarized EMWs at $n = 1$, $\varphi^{-}_{p(\max)} = -3.06°$ at $\theta_p = 67.93°$ the transmission coefficient is high: $T_p = 0.919$. The maximum positive rotation $\varphi^{-}_{p(\max)} = 0.362°$ occurs at $\theta_s = 45.8°$ but the transmission coefficient is low: $T_s = 0.129$. At the sixth peak $T_p = 0.999$ the value $\varphi_P = -1.61°$ is reached.

Triple thickening of the magnetic layers $(n = 3)$ gives for *s*-polarized wave $\varphi^{-}_{s(\max)} = -24.85°$ at low transmission coefficient $T_s = 0.101$. But at the fifth transmission peak $T_s = 0.997$ the FR $\varphi_s = -7.31°$ is reached at $\theta_s = 43.5°$. For the *p*-polarization case, the maximal negative value $\varphi^{-}_{p(\max)} = -13.2°$ occurs at $\theta_p = 45.42°$ with a high transmission coefficient: $T_p = 0.804$.

With further thickening of the magnetic layers up to $n = 5$ for *s*-polarized wave we obtain $\varphi^{-}_{s(\max)} = -41.78°$ at low transmission coefficient $T_s = 0.191$. But at the sixth peak at $T_s = 0.946$ we get large FR $\varphi_s = -20.25°$ at $\theta_s = 34.4°$. In the case of *p*-polarization, the maximum FR $\varphi^{-}_{p(\max)} = -24.29°$ is reached with good transmission: $T_p = 0.814$ and at the fifth transmission coefficient peak at $T_p = 0.911$ the FR is $\varphi_p = -13.78°$.

In Fig. 6, the spectra of FR $\varphi_s(\omega, \theta)$ (*a*) and $\varphi_p(\omega, \theta)$ (*b*) for the structure $[(SY)^3(TB)^5]^7$ with quintuple thickened YIG and Bi:YIG magnetic layers in the regions of intra-PBG passbands corresponding to *s*- and *p*-polarized incident EMWs (near $\lambda_0 = 1.55\,\mu\text{m}$ $(\omega_0 \approx 1.215\,\text{rad·PHz})$) show the following features. As seen in Fig. 6, *a*, the strongest negative FR occurs for *s*-polarized radiation at the low-frequency edge of the transmission band: $\varphi_s \sim (-40 \div -30°)$. At the high-frequency edge of the passband, depending on the incidence angle θ, the FR φ_s can take both negative and positive values within ±5°. For *p*-polarized EMWs, the largest positive rotation φ_p (a few degrees) is achieved either at the high-frequency passband edge or (with increasing θ) at points shifted from it towards the center of the band. Unlike the *s*-polarization case, the sharp negative extremum about $\varphi_p \sim (-25 \div -20°)$ is not at the high-frequency edge but at frequencies slightly shifted from the edge towards the band center (Fig. 6, *b*).

For wavelength $\lambda_0 = 1.3\,\mu\text{m}$ in the case of quintuple thickened magnetic layers in $[(SY)^3(TB)^5]^7$ calculations show good agreement of the FR maxima and the transmission coefficients. There are two angular intervals: $0 < \theta < 25°$ and $30 < \theta < 65°$, separated by PBG regions.

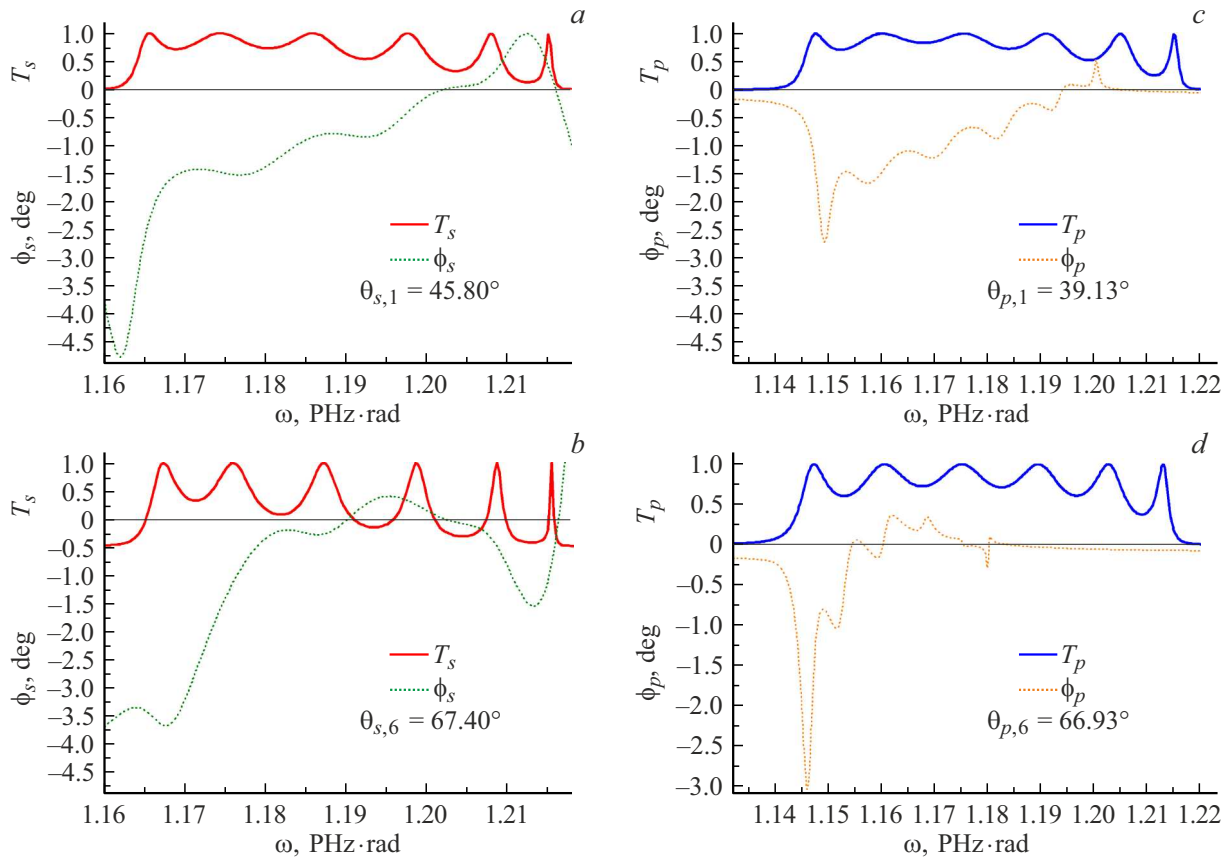

Figure 4. Frequency dependencies of the transmission coefficients and FR angles for s-polarized EMWs ($T_s(\omega)$, $\varphi_s(\theta)$) at the incidence angles $\theta_{s1} = 45.80°$ (a), $\theta_{s6} = 67.40°$ (b) and p-polarized EMWs ($T_p(\omega)$, $\varphi_p(\theta)$) at $\theta_{p1} = 39.13°$ (c), $\theta_{p6} = 66.93°$ (d). The frequency intervals correspond to the second intraband transmission band.

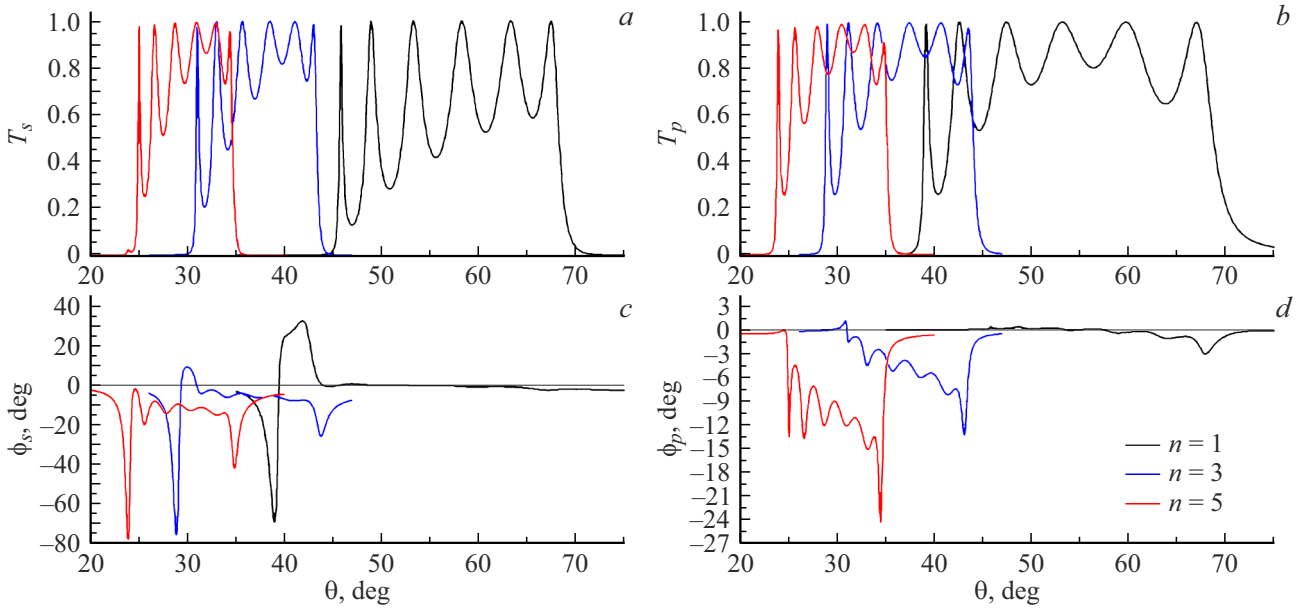

Figure 5. Evolution of the angular dependence of transmission coefficients $T_s(\theta)$ (a), $T_p(\theta)$ (b) and FR angles$\varphi_s(\theta)$ (c), $\varphi_p(\theta)$ (d) for PC $[(SY)^3(TB)^5]^7$ at $\lambda_0 = 1.55\,\mu$m ($\omega_0 \approx 1.215$ rad·PHz) at n-fold variation in the thicknesses of magnetic layers $d_Y = n\,d_{0Y}$, $d_B = n\,d_{0B}$, ($n = 1, 3, 5$). Here $d_{0Y} = 0.1760\,\mu$m, $d_{0B} = 0.1615\,\mu$m.

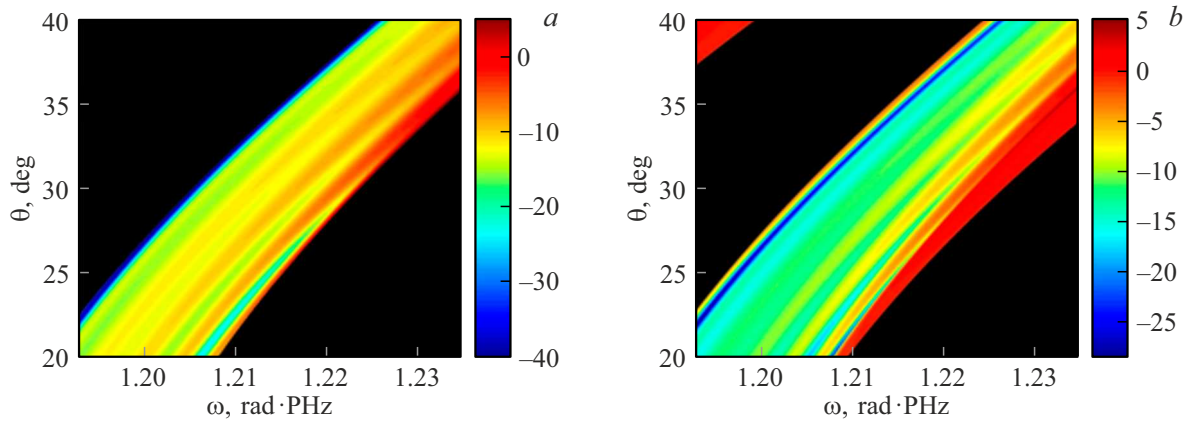

Figure 6. spectra of the FR $\varphi_s(\omega,\theta)$ (a) and $\varphi_p(\omega,\theta)$ (b) for the structure $[(SY)^3(TB)^5]^7$ with quintuple thickened magnetic layers YIG and Bi:YIG: $d_Y = 5d_{0Y} = 0.8800\,\mu$m, $d_B = 5d_{0B} = 0.8075\,\mu$m. Black regions correspond to negligibly small transmission coefficients: $T_s(\omega,\theta) \to 0$ (a) and $T_p(\omega,\theta) \to 0$ (b), i.e., they indicate the PBGs regions. The color scale represents FR angles in degrees.

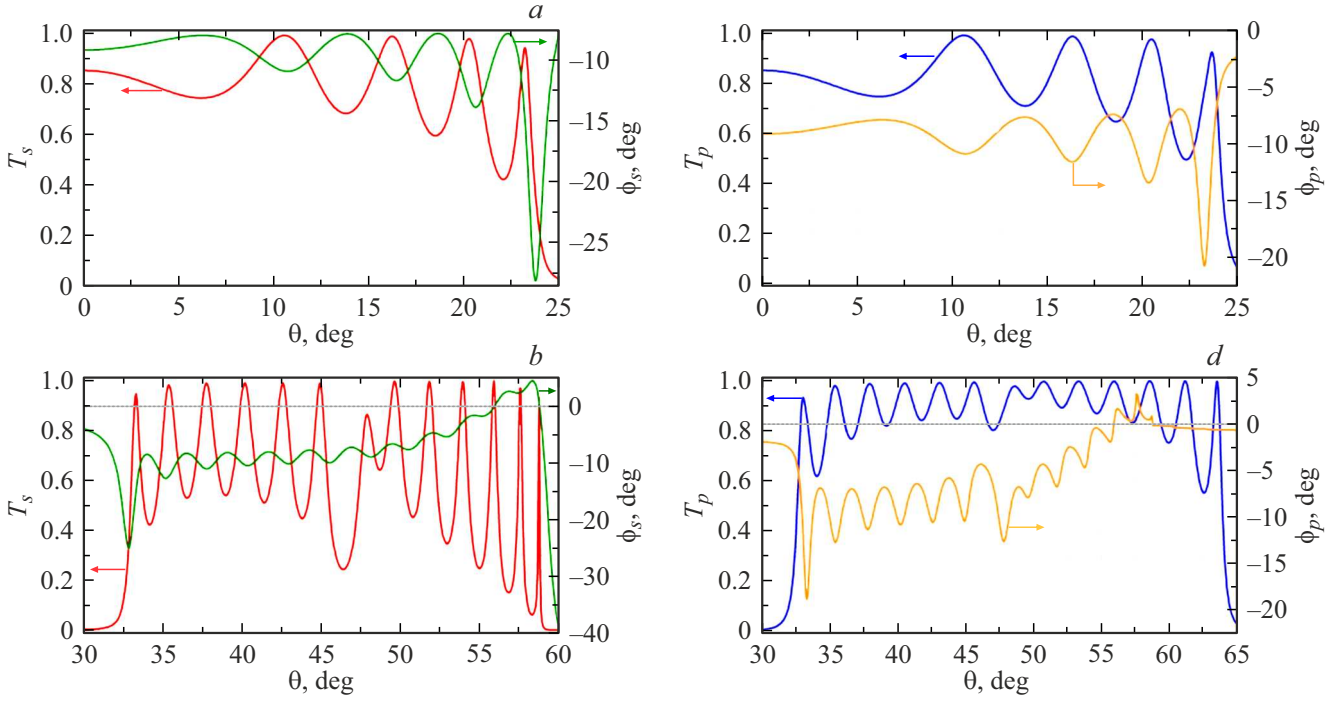

Figure 7. Angular dependencies of the transmission coefficients and FR angles: $T_s(\theta)$ and $\varphi_s(\theta)$ (a,c); $T_p(\theta)$ and $\varphi_p(\theta)$ (b,d) at $\lambda = 1.3\,\mu$m $(\omega_0 \approx 1.449\,\text{rad}\cdot\text{PHz})$ for the structure $[(SY)^3(TB)^5]^7$ with thickened magnetic layers YIG and Bi:YIG: $d_Y = 5d_{0Y} = 0.8800\,\mu$m, $d_B = 5d_{0B} = 0.8075\,\mu$m. Red and blue curves correspond to transmission coefficients, green and orange — FR angles.

The first interval, shown in Fig. 7, a for s-polarized waves, at high transmission coefficients $T_s = 0.976$ (at $\theta_s = 16.42°$) and $T_s = 0.904$ (at $\theta_s = 20.58°$) the Faraday angles are $\varphi_s = -11.63°$ and $\varphi_s = -13.81°$ respectively. In this case, the maximum FR for the s-polarized wave $\varphi^-_{s(\max)} = -28.05°$ occurs at $\theta_s = 23.75°$ and $T_s = 0.334$. For p-polarized EMWs (Fig. 7, b), the maximum negative value $\varphi^-_{p(\max)} = -20.74°$ at $\theta_p = 23.25°$ with the transmission coefficient $T_p = 0.762$. Other maxima coincide as well, e.g., $\varphi^-_{p(\max)} = -13.43°$ (at $\theta_p = 20.33°$) and $T_p = 0.967$ (Fig. 7, b). The second interval, shown in Fig. 7, c, d, corresponds to the PBG edge, where the maximum FR for s-polarized EMWs is $\varphi^-_{s(\max)} = -25.13°$ $(\theta_s = 32.86°)$, $T_s = 0.339$. Over a relatively wide range of incidence angles $(33.8 < \theta_p < 49.0°)$ the FR varies within $-13 < \varphi_p < -7°$ with transmission $0.43 < T_p < 0.99$. For p-polarized waves (Fig. 7, d), the maximal negative FR reaches $\varphi^-_{p(\max)} = -18.78°$ at high transmission $T_p = 0.8516$ $(\theta_p = 33.27)$. Most other FR peaks lie within $-14 < \varphi^-_p < -7°$ $(33.5 < \theta_p < 49.8°)$,

corresponding to high transmission coefficients within $0.62 < T_p < 0.97$.

Note that the 180-degree magnetization reversal of the PC structure changes the FR sign. This allows achieving the same absolute values but positive FRs $\varphi_s \sim (30-40^\circ)$ and $\varphi_s \sim (20-25^\circ)$ for the same EMW polarizations, frequencies, and incidence angles.

Although the coincidence of spectral maxima of the optical transmission and large Faraday angles is not a unique effect, it remains relatively rare in the examined wavelength range (near-IR). Such coincidences of maximum transmission values with giant FR angles in various single-periodic PCs with defect layers were described in works [18,29,30,44]. For example, in [30] on PC structures $(SiO_2/TiO_2)^k$/BiYIG/$(TiO_2/SiO_2)^k$ numerical FR with specific values $-28^\circ/\mu$m was obtained. However, these giant values occur at very low ($\sim 2\%$) transmission. Good transmission ($\sim 73\%$ and $\sim 87\%$) accompanies specific rotations $-1^\circ/\mu$m and $-0.83^\circ/\mu$m respectively, with average transmission coefficient ($\sim 42\%$) corresponding to FR $-2.8^\circ/\mu$m [30]. Calculations done in [44] for magnetic PCs based on GGG and Bi:YIG with two (magnetic and non-magnetic) defect layers showed that under certain structure parameters, specific FR reaches $2-4.8^\circ/\mu$m at high transmission coefficients (0.95–0.98). Work [18] presented theoretical FR calculations on a 1D PC $(SiO_2/GGG)^N$/ Bi:YIG/$(GGG/SiO_2)^N$ containing a magnetic defect. With some defect layer thickness and period number combinations, specific FR values up to several degrees per micron were obtained: $\Phi \sim -1.5^\circ/\mu$m (at $T_p \sim 0.9$), $\Phi \sim -3^\circ/\mu$m (at $T_p \sim 0.5$). The highest value $\Phi \sim -6^\circ/\mu$m corresponds to a small transmission $T_p \sim 0.1-0.15$. In [29], giant FR was experimentally observed in PCs with complex magnetic defects (two different Bi:YIG layers) of the form $(TiO_2/SiO_2)^m$/M/$(SiO_2/TiO_2)^m$. In the visible wavelength range 613–761 nm specific rotations up to $66^\circ/\mu$m were reached at $T = 0.6$ ($\theta_F = -20.3^\circ$).

Typically, defect-free periodic PCs do not exhibit such high FR values, and noticeable Faraday rotation appears at low EMW transmission coefficients. For example, in a two-periodic (photonic-magnonic) crystal [YIG /$(TiO_2/SiO_2)^4$/TiO_2]^5 studied in [12], the maximum specific FR values for *s*- and *p*-polarized waves were $\varphi^{\pm}_{s(\max)} = -1.5^\circ$ ($T_s \sim 0.02$) and $\varphi^{-}_{p(\max)} = -0.3^\circ$ ($T_p \sim 0.15$), respectively, which, considering the total PC thickness, gave specific rotation values of about $\Phi_s = \pm 0.11^\circ/\mu$m and $\Phi_p = -0.02^\circ/\mu$m. Near-unity transmission corresponded to very small FR: $\varphi_s \sim 0.01^\circ$, $\varphi_s \sim 0.03^\circ$.

In this work, we demonstrate the possibility of achieving sufficiently large FR values (from several degrees to tens of degrees) with significant transmission precisely in the defect-free periodic structure. In the PC $[(SY)^3(TB)^5]^7$, having a total length $L_s = 20.511\,\mu$m, the specific FR at wavelength $\lambda_0 = 1.3\,\mu$m reaches the highest values $\Phi_p = -0.233^\circ/\mu$m ($\varphi^{-}_{p(\max)} = -4.78^\circ$, $T_p = 0.71$) and $\Phi_s = -0.21^\circ/\mu$m ($\varphi^{-}_{s(\max)} = -4.2^\circ$, $T_p = 0.79$). For wavelength $\lambda_0 = 1.55\,\mu$m the corresponding specific values are $\Phi_p = -0.15^\circ/\mu$m ($\varphi^{-}_{p(\max)} = -3.05^\circ$, $T_p = 0.82$) and $\Phi_s = -0.11^\circ/\mu$m ($\varphi^{-}_{s(\max)} = -2.3^\circ$, $T_s = 0.9$). For PCs with fivefold increased magnetic layer thicknesses ($L_s = 57.903\,\mu$m) the highest specific FR values at wavelength $\lambda_0 = 1.55\,\mu$m are: $\Phi_p = -0.72^\circ/\mu$m ($\varphi^{-}_{p(\max)} = -41.78^\circ$, $T_p = 0.19$), $\Phi_p = -0.42^\circ/\mu$m ($\varphi^{-}_{p(\max)} = -24.29^\circ$, $T_p = 0.81$) and $\Phi_s = -0.32^\circ/\mu$m ($\varphi^{-}_{s(\max)} = -20.25^\circ$, $T_p = 0.946$). At wavelength $\lambda_) = 1.3\,\mu$m the highest specific FR values are$\Phi_s = -0.49^\circ/\mu$m ($\varphi^{-}_{s(\max)} = -28.05^\circ$, $T_p = 0.34$) and$\Phi_p = 0.36^\circ/\mu$m ($\varphi^{-}_{p(\max)} = -20.74^\circ$, $T_p = 0.762$). These specific FR values are comparable with theoretical results obtained in [11] for two PC structures based on SiO_2 and Ta_2O_5 with complex magnetic defects from Bi:YIG and SiO_2 layers, where specific FR reach $0.446^\circ/\mu$m and $0.676^\circ/\mu$m at transmission coefficients close to unity. In the case of the three-periodic photonic crystal (PC) $[(SY)^3(TB)^5]^7$ the obtained specific FR values are several times smaller than those in work [18], but they exceed by one to two orders of magnitude the corresponding values of FR in two-periodic magnetic PCs [12].

Conclusion

In this work, we have shown that in a one-dimensional defect-free three-periodic PC based on layers of silicon and titanium oxides, as well as magnetic layers of ferrite garnets YIG and Bi:YIG, it is possible to combine high (close to unity) transmission coefficients and large Faraday rotation angles (up to several tens of degrees) in intraband pass regions close to telecommunications wavelengths $\lambda_0 = 1.55\,\mu$m and $\lambda_0 = 1.3\,\mu$m.

The values of Faraday rotation angles for the structure $(SiO_2/YIG)^3(TiO_2/Bi:YIG)^5]^7$ at certain frequencies can significantly (by one–to two orders of magnitude) exceed the values for magnonic-photonic crystals of the type [YIG/$(TiO_2/SiO_2)^4$]^5/YIG [12]. Moreover, in the three-period PC, the maxima of Faraday rotation for *s*- and *p*-polarized waves can coincide with corresponding regions of high transmission. Thus, at fixed angles of incidence, tuning the frequency within the passband allows achieving good results — significant Faraday rotations at maximal electromagnetic wave transmission.

The possibility of polarization tuning (switching the polarization of incident electromagnetic waves) of the Faraday rotation angle and transmission coefficients is demonstrated, as well as tuning these parameters by changing the angle of incidence of infrared radiation. For both wavelengths ($\lambda_0 = 1.55\,\mu$m and $\lambda_0 = 1.3\,\mu$m) Faraday angles can reach comparable values at sufficiently high ($> 70\%$) transmission, i.e., the structure can function at two operating frequencies.

The presented results indicate the promise of using multi-periodic magneto-photonic crystals for potential technical developments of optoelectronics and nanophotonics devices. It should also be noted that similar to the photonic crystals considered in [10–12], three-periodic photonic crystals with magnetic layers, in particular photonic crystals of the type $[(ST)^N(YB)^M]^K$, can act as complex magnonic crystals capable of supporting and transmitting gigahertz-range magnon excitations independently of electromagnetic waves. According to our estimates, in the structure $[(ST)^N(YB)^M]^K$ the Faraday rotation can reach -63° at moderate electromagnetic wave transmission. Considering this feature, such three-periodic systems can be used as multifunctional structures (magnonic-photonic crystals) with forbidden magnon and photon bands in the gigahertz and petahertz ranges, respectively, which can form the basis of new multifunctional devices at the intersection of photonics and magnonics.

Funding

This study was supported by the Russian Science Foundation, project № 23-22-00466).

Conflict of interest

The authors declare that they have no conflict of interest.

References

[1] A.K. Zvezdin, V.A. Kotov. *Modern Magnetooptics and Magnetooptical Materials* (Bristol, Institute of Physics Publishing, 1997). DOI: 10.1201/9780367802608
[2] *Magnetism*, ed. by É. Du Trémolet de Lacheisserie, D. Gignouxand M. Schlenker (Boston, Springer, 2005).
[3] J. Grafe, M. Schmidt, P. Audehm, G. Schutz, E. Goering. Rev. Sci. Instrum., **85**, 023901 (2014). DOI: 10.1063/1.4865135
[4] M. Atatüre, J. Dreiser, A. Badolato, A. Imamoglu. Nature Phys., **3**, 101 (2007). DOI: 10.1038/nphys521
[5] N. Dissanayake, M. Levy, A. Chakravarty, P.A. Heiden, N. Chen, V.J. Fratello. J. Appl. Phys., **99**, 091112 (2011). DOI: 10.1063/1.3633344
[6] Y.S. Dadoenkova, I.L. Lyubchanskii, Y.P. Lee, T. Rasing. Appl. Phys. Lett., **97** (11), 011901 (2010). DOI: 10.1063/1.3488679
[7] T. Goto, A.V. Baryshev, K. Tobinaga, M. Inoue. J. Appl. Phys., **107**, 09A946 (2010). DOI: 10.1063/1.3365431
[8] T. Mikhailova, A. Shaposhnikov, A. Prokopov, A. Karavainikov, S. Tomilin, S. Lyashko, V. Berzhansky. In: *EPJ Web of Conferences* (2018), vol. 185, 02016. DOI: 10.1051/epjconf/201818502016
[9] Y.S. Dadoenkova, F.F.L. Bentivegna, S.G.Moiseev. Phys. Scr., **98**, 105006 (2019). DOI: 10.1088/1402-4896/ab2780
[10] E.A. Diwan, F. Royer, D. Jamon, R. Kekesi, S. Neveau, M.F. Blanc-Mignon, J.J. Rousseau. JNN, **16**, 10160 (2016). DOI: 10.1166/jnn.2016.12844
[11] B. Gaiyan, D. Lijuan, F. Shuai, F. Zhifang. Opt. Mater., **35** (2), 252 (2012). DOI: 10.1016/j.optmat.2012.08.015
[12] Y.S. Dadoenkova, N.N. Dadoenkova, I.L. Lyubchanskii, J. Klos, M. Krawczyk. IEEE Trans. Magn., **53**, 2501005 (2017). DOI: 10.1109/TMAG.2017.2712278
[13] J.W. Klos, M. Krawczyk, Y.S. Dadoenkova, N.N. Dadoenkova, I.L. Lyubchanskii. J. Appl. Phys., **115** (17), 174311 (2014). DOI: 10.1063/1.4874797
[14] Y.S. Dadoenkova, N.N. Dadoenkova, I.L. Lyubchanskii, J.W. Klos, M. Krawczyk. J. Appl. Phys., **120** (7), 73903 (2016). DOI: 10.1063/1.4961326
[15] J.W. Klos, M. Krawczyk, Y.S. Dadoenkova, N.N. Dadoenkova, I.L. Lyubchanskii. IEEE Trans. Magn., **50** (11), 2 (2014). DOI: 10.1109/TMAG.2014.2321532
[16] Y.S. Dadoenkova, N.N. Dadoenkova, J.W. Kłos, M. Krawczyk, I.L. Lyubchanskii. Phys. Rev. A, **96** (4), 43804 (2017). DOI: 10.1103/PhysRevA.96.043804
[17] J.D. Joannopoulos, S.G. Johnson, J.N.J. Winn, R.D. Meade. *Photonic Crystals. Molding the Flow of Light*, 2nd ed. (Princeton, Prinstone University Press, 2008).
[18] S.V. Eliseeva, Y.F. Nasedkina, D.I. Sementsov. Progr. Electromag. Res. M, **51**, 131 (2016). DOI: 10.2528/PIERM16080403
[19] I.S. Panyaev, L.R. Yafarova, D.G. Sannikov, N.N. Dadoenkova, Y.S. Dadoenkova, I.L. Lyubchanskii. J. Appl. Phys., **126** (10), 103102 (2019). DOI: 10.1063/1.5115829
[20] I.S. Panyaev, N.N. Dadoenkova, Y.S. Dadoenkova, I.A. Rozhleys, M. Krawczyk, I.L. Lyubchanskii, D.G. Sannikov. J. Phys. D, **49** (43), 435103 (2016). DOI: 10.1088/0022-3727/49/43/435103
[21] I.S. Panyaev, D.G. Sannikov, Y.S. Dadoenkova, N.N. Dadoenkova. IEEE Sens. J., **22** (23), 22428 (2022). DOI: 10.1109/JSEN.2022.3217117
[22] I.S. Panyaev, D.G. Sannikov, N.N. Dadoenkova, Y.S. Dadoenkova. Appl. Opt., **60** (7), 1943 (2021). DOI: 10.1364/ao.415966
[23] I.A. Glukhov, S.G. Moiseev. Opt. Spetrosk., **131** (11), 1475 (2023). DOI: 10.61011/OS.2023.11.57005.5095-23
[24] A.D. Block, P. Dulal, B.J.H. Stadler, N.C.A. Seaton. IEEE Photonics J., **6**, 0600308 (2014). DOI: 10.1109/JPHOT.2013.2293610
[25] A. Kehlberger, K. Richter, M.C. Onbasli, G. Jakob, D.H. Kim, T. Goto, C.A. Ross, G. Gotz, G. Reiss, T. Kuschel, M. Klaui. Phys. Rev. Applied, **4**, 014008 (2015). DOI: 10.1103/PhysRevApplied.4.014008
[26] S. Mito, Yu. Shiotsu, J. Sasano, H. Takagi, M. Inoue. AIP Advances, **7** (5), 056316 (2017). DOI: 10.1063/1.4976952
[27] F. Royer, B. Varghese, E. Gamet, S. Neveau, Y. Jourlin, D. Jamon. ACS Omega, **5**, 2886 (2020). DOI: 10.21/acsomega.9b03728
[28] T.V. Mikhailova, V.N. Berzhansky, A.N. Shaposhnikov, A.V. Karavainikov, A.R. Prokopov, Y.M. Kharchenko, I.M. Lukienko, O.V. Miloslavskaya, M.F. Kharchenko. Opt. Mater., **78**, 521 (2018). DOI: 10.1016/j.optmat.2018.03.011
[29] V.N. Berzhansky, A.N. Shaposhnikov, A.R. Prokopov, A.V. Karavainikov, T.V. Mikhailova, I.N. Lukienko, Yu.N. Kharchenko, V.O. Golub, O.Yu. Salyuk, V.I. Belotelov, ZhETF, **150**, 859 (2016). (in Russian) DOI: 10.7868/S004445101611002X
[30] M. Inoue, K.I. Arai, T. Fujii, M. Abe. J. Appl. Phys., **83** (11), 6768 (1998). DOI: 10.1063/1.367789
[31] M. Inoue, R. Fujikawa, A. Baryshev, A. Khanikaev, P.B. Lim, H. Ushida, O. Aktsipetrov, A. Fedyanin, T. Murzina, A. Granovsky. J. Phys. D, **39**, R151 (2006). DOI: 10.1109/INTMAG.2006.375428
[32] D.O. Ignatyeva, T.V. Mikhailova, P. Kapralov, S. Lyashko, V.N. Berzhansky, V.I. Belotelov. Phys. Rev. Applied, **22** (4), 044064 (2024). DOI: 10.1103/PhysRevApplied.22.044064

[33] I.A. Glukhov, I.S. Panyaev, D.G. Sannikov, Yu.S. Dadoenkova, N.N. Dadoenkova. Opt. i spektr., **132** (5), 557 (2024) (in Russian). DOI: 10.61011/OS.2024.05.58464.6401-24
[34] D.W. Berreman. J. Opt. Soc. Am., **62** (4), 502 (1972). DOI: 10.1364/JOSA.62.000502
[35] J.R. Devore. J. Opt. Soc. Am., **41** (6), 416 (1951). DOI: 10.1364/JOSA.41.000416
[36] I.H. Malitson. J. Opt. Soc. Am., **55** (10), 1205 (1965). DOI: 10.1364/JOSA.55.001205
[37] B. Johnson, A.K. Walton. Br. J. Appl. Phys., **16** (4), 475 (1965). DOI: 10.1088/0508-3443/16/4/310
[38] M. Torfeh, H. Le Gall. Phys. Status Solidi, **63** (1), 247 (1981). DOI: 10.1002/pssa.2210630133
[39] V. Doormann, J.P. Krumme, C.P. Klages, M. Erman. Appl. Phys. A, **34** (4), 223 (1984). DOI: 10.1007/BF00616576
[40] M. Wallenhorst, M. Niemöller, H. Dötsch, P. Hertel, R. Gerhardt, B. Gather. J. Appl. Phys., **77** (7), 2902 (1995). DOI: 10.1063/1.359516
[41] J.P. Krumme, C.P. Klages, V. Doormann. Appl. Opt., **23** (8), 1184 (1984). DOI: 10.1364/AO.23.001184
[42] N.N. Dadoenkova, I.L. Lyubchanskii, M.I. Lyubchanskii, E.A. Shapovalov, Y.P. Lee. *Frontiers in Optical Technology: Materials & Devices* (Nova Science, New York, 2007), p. 22–72.
[43] V.I. Belotelov, A.K. Zvezdin. Photonic Crystals and Other Metamaterials (Bureau Quantum, Moscow, 2006) 143 pages. (in Russian)
[44] M.J. Steel, M. Levy, R.M. Osgood, Jr. IEEE Photonics Technology Letters, **12** (9) 1171 (2000). DOI: 10.1109/68.874225

Translated by J.Savelyeva